Communications in Physics, Vol. 29, No. 4 (2019), pp. 455-470
DOI:10.15625/0868-3166/29/4/13818

REAL-SPACE APPROACH FOR THE ELECTRONIC CALCULATION OF TWISTED BILAYER GRAPHENE USING THE ORTHOGONAL POLYNOMIAL TECHNIQUE

HOANG ANH LE[1], VAN THUONG NGUYEN[1], VAN DUY NGUYEN[1], VAN-NAM DO[1,†] AND SI TA HO[2]

[1]*Phenikaa Institute for Advanced Study,*
C1 building, Phenikaa University, Yen Nghia ward, Ha Dong district, Hanoi, Vietnam
[2]*National University of Civil Engineering, 55 Giai Phong road, Hanoi, Vietnam*

[†]*E-mail:* nam.dovan@phenikaa-uni.edu.vn

Received 16 May 2019
Accepted for publication 29 November 2019
Published 12 December 2019

Abstract. *We discuss technical issues involving the implementation of a computational method for the electronic structure of material systems of arbitrary atomic arrangement. The method is based on the analysis of time evolution of electron states in the real lattice space. The Chebyshev polynomials of the first kind are used to approximate the time evolution operator. We demonstrate that the developed method is powerful and efficient since the computational scaling law is linear. We invoked the method to study the electronic properties of special twisted bilayer graphene whose atomic structure is quasi-crystalline. We show the density of states of an electron in this graphene system as well as the variation of the associated time auto-correlation function. We find the fluctuation of electron density on the lattice nodes forming a typical pattern closely related to the typical atomic pattern of the quasi-crystalline bilayer graphene configuration.*

Keywords: bilayer; Chebyshev polynomials; electronic structure; graphene; quasi-crystalline; time evolution.

Classification numbers: 73.22.Pr; 71.15.-m; 31.15.X-.

I. INTRODUCTION

Twisted bilayer graphene (TBG) is an engineered material, which can be formed by stacking two graphene layers on each other using the transfer technique. By this method, the two graphene lattices are generally mismatched. The lattice alignment is characterized by a twist angle

and a displacement between the two layers. In this system, the van der Waals interaction governs the coupling of two graphene layers and keeps the TBG configurations stable [1, 2]. In general, stacking two material layers permits to exploit the interlayer coupling and the lattice alignment between the two constituent lattices to manipulate the electronic properties of this composed system. It was predicted that twisting two graphene layers allows a strong tuning of its electronic properties. Many van Hove singularity peaks were observed in the electronic energy spectrum [3–7]. Especially, a very narrow band containing the intrinsic Fermi energy level in some special TBG configurations was considered to support the dominance of many-body physics [8–12]. It was experimentally demonstrated by Cao *et al.* that the TBG configuration with the twist angle of 1.08° exhibits several strongly correlated phases, including an unconventional superconducting and a Mott-like phase [13, 14].

A generic stacking two material layers imply that the alignment between the two constituent lattices is not always guaranteed to be commensurate. The atomic configurations of TBGs can be characterized by an in-plane vector $\boldsymbol{\tau}$ and a twist angle θ defining, respectively, the relative shift and rotation between the two graphene lattices. It is, however, shown that, regardless of τ, when $\theta = \text{acos}[(3m^2+3mr+r^2/2)/(3m^2+3mr+r^2)]$, in which m, r are coprime integers, the stacking is commensurate [4, 15–19]. Though the translational symmetry of the TBG lattice is preserved in this case, a large unit cell is usually defined, especially for small twist angles θ. Conventional methods based on the time-independent Schrodinger equation associated with the Bloch theorem are commonly used to calculate the electronic structure. Such methods, unfortunately, are not applicable for the incommensurate TBG lattices because of the loss of the translational invariance. Partial knowledge on the energy spectrum, however, can be obtained by interpolating/extrapolating data of the energy spectrum of commensurate TBG configurations for that of the incommensurate ones. This scheme is guaranteed by a demonstration of the continuous variation of the energy spectrum versus the twist angle [20]. Effective continuum models can be also constructed to study the electronic structure of TBG configurations of tiny twist angles [3, 5, 7, 15, 21–23].

In this work, we will demonstrate that the electronic structure of a generic atomic lattice, with or without the translational symmetry, can be obtained efficiently by using the real-space approach, instead of the reciprocal space approach. The method we developed is based on the analysis of the dynamics of electrons in an atomic lattice. There are many technical issues involving the implementation of this method. In this article, we will address such technical issues in details. We rigorously validate the method and then present the calculated data of the electronic properties of a special incommensurate TBG configuration with the twist angle of 30°. Depending on the choice of the twist axis, the resulted atomic lattice can possess a rotational symmetry axis. Specifically, by starting from the AA-stacking configuration, if the twist axis (perpendicular to the lattice plane) goes through the position of a carbon atom, it is the 3-fold axis. However, if the twist axis goes through the central point of the hexagonal ring, it is the 12-fold axis. The latter choice is special because it is not only a higher-order symmetry axis but the resulted TBG configuration is a particular quasi-crystal, see Fig. 1 [24, 25]. Very recently, the electronic structure of this system was interested in [26]. However, the investigation was based on an effective model describing 12-fold symmetric resonant electronic states and/or on the extrapolation of the data of a close commensurate TBG configuration, *e.g.,* $\theta = 29.99^\circ$. Such a method is clearly different from, and not natural as our developed approach. On the basis of the developed method, we are able to calculate not only the local density of states (LDOS), the total density of states (DOS), but

also the distribution of electron density on the lattice nodes. We find that the distribution of the electron density fluctuation shows a typical pattern, which is consistent with the symmetry of the atomic lattice.

The outline of this paper is as follows. In Sec. II, we present in details the basis of the calculation method and an empirical tight-binding model which allows characterizing the dynamics of the $2p_z$ electrons in the TBG atomic lattices. Particularly, we show in Sub-sec. II.1 how the formula of the density of states is reformulated in terms of a time auto-correlation function, which is determined from a set of intermediate Chebyshev states established from recursive relations. We review the essence of a stochastic technique to evaluate the trace of Hermitian operators in Sub-sec. II.2. Especially, we present in Sub-sec. II.3 an algorithm for sampling lattice nodes to define initial electronic states. In Sec. III, we first discuss important computational issues involving the implementation of the method and then present results for the density of states and the distribution of the valence electron density on interested TBG configurations. Finally, we present conclusions in Sec. IV.

II. THEORY

II.1. Chebyshev states and calculation of density of states

The density of states — the number of electron states whose energies are in the vicinity of given energy value and measured in a unit of space volume — is a basic quantity characterizing the energy spectrum of an electronic system. Denoting $\{E_n\}$ and $\{|n\rangle\}$ the eigenvalues and eigenvectors of a Hamiltonian $\hat{\mathscr{H}}$ that describes the dynamics of an electron system, DOS is formulated as follows:

$$\rho(E) = \frac{s}{\Omega_a}\sum_n \delta(E-E_n) = \frac{s}{\Omega_a}\sum_n \langle n|\delta(E-\hat{\mathscr{H}})|n\rangle, \tag{1}$$

where s is the factor accounting for the degeneracy of some degrees of freedom such as spin and/or valley, Ω_a is a volume used to normalise DOS. Eq. (1) is rewritten in the general form:

$$\rho(E) = \frac{s}{\Omega_a}\mathrm{Tr}\left[\delta(E-\hat{\mathscr{H}})\right], \tag{2}$$

where the symbol "Tr[...]" denotes the trace of operator inside. This equation is very instructive because it suggests the use of different representation to evaluate the trace. Since the operator $\delta(E-\hat{\mathscr{H}})$ is an abstract form, we would go further by using the formal formula

$$\delta(E-\hat{\mathscr{H}}) = \frac{1}{2\pi\hbar}\int_{-\infty}^{+\infty} dt e^{iEt/\hbar}\hat{\mathscr{U}}(t), \tag{3}$$

where $\hat{\mathscr{U}}(t) = \exp\left(-i\hat{\mathscr{H}}t/\hbar\right)$ is nothing rather than the definition of the time evolution operator. Substitute (3) into (2) we obtain this formula for DOS:

$$\rho(E) = \frac{s}{\pi\hbar\Omega_a}\mathrm{Re}\left\{\int_0^{+\infty} dt e^{iEt/\hbar}C(t)\right\}, \tag{4}$$

where the symbol "Re" denotes taking the real part of the integral value, and the function $C(t)$ is defined by

$$C(t) = \mathrm{Tr}\left[\hat{\mathscr{U}}(t)\right]. \tag{5}$$

Eq. (4) tells us that the density of states of an electron is the power spectrum of $C(t)$ that, as will be seen in subsection II.3, is truly a time auto-correlation function.

The exponential form of $\hat{\mathscr{U}}(t)$ is useful because it suggests that we can use the Taylor expansion to specify this operator. Practically, concerning the convergent issue of the expansion, orthogonal polynomials should be used instead. In our work, we use Chebyshev polynomials of the first kind $Q_m(x) = \cos[m\arccos(x)]$ to expand $\hat{\mathscr{U}}(t)$ [27]. Though defined through a geometrical function, $Q_m(x)$ are truly polynomials,

$$\begin{aligned} Q_0(x) &= 1, \\ Q_1(x) &= x, \\ Q_2(x) &= 2x^2 - 1, \\ Q_3(x) &= 4x^3 - 3x, \\ &\vdots \\ Q_m(x) &= 2xQ_{m-1}(x) - Q_{m-2}(x), \end{aligned} \tag{6}$$

where x is defined in the range of $[-1,1]$. These expressions can be simply obtained from the formal definition of $Q_m(x)$. The two first equations and the last one compose the recursive relation of the Chebyshev polynomials of the first kind. For the sake of using $Q_m(x)$ for the expansion of a function, it is useful to notice their orthogonal relationship. Indeed, the Chebyshev polynomials are orthogonal via the weight of $1/\pi\sqrt{1-x^2}$. Particularly, we have:

$$\int_{-1}^{1} dx \frac{1}{\pi\sqrt{1-x^2}} T_m(x)T_n(x) = \frac{\delta_{m,0}+1}{2}\delta_{m,n}, \tag{7}$$

where $\delta_{m,n}$ is the conventional Kronecker symbol.

In order to apply the polynomials $Q_m(x)$ in the development of $\hat{\mathscr{U}}(t)$ we first need to rescale the spectrum of Hamiltonian $\hat{\mathscr{H}}$ to the interval $[-1,1]$. This scaling is obtained by replacing $\hat{\mathscr{H}}$ by a rescaled one $\hat{h}$ via the transformation $\hat{\mathscr{H}} = W\hat{h} + E_0$, wherein W is the half of spectrum bandwidth, E_0 the central point of the spectrum. It is now straightforward to write the time-evolution operator in terms of the Chebyshev polynomials as follows:

$$\hat{\mathscr{U}}(t) = e^{iE_0t/\hbar} \sum_{m=0}^{+\infty} \frac{2}{\delta_{m,0}+1} (-i)^m B_m\left(\frac{Wt}{\hbar}\right) Q_m(\hat{h}), \tag{8}$$

where B_m is the m-order Bessel function of the first kind. Besides the time-evolution operator, we also have the expression of the delta operator $\delta(E-\hat{\mathscr{H}})$ and the step operator $\theta(E-\hat{\mathscr{H}})$ in terms of the Chebyshev polynomials as follows:

$$\delta(E-\hat{\mathscr{H}}) = \frac{\theta(1-\epsilon)\theta(1+\epsilon)}{W\pi\sqrt{1-\epsilon^2}} \sum_{m=0}^{+\infty} \frac{2}{\delta_{m,0}+1} Q_m(\epsilon)\, Q_m(\hat{h}), \tag{9}$$

where $\epsilon = (E-E_0)/W$, and

$$\theta(E-\hat{\mathscr{H}}) = \theta(1-\epsilon)\theta(1+\epsilon) \sum_{m=0}^{+\infty} \frac{2}{\delta_{m,0}+1} \frac{\sin[m\arccos(\epsilon)]}{m\pi} Q_m(\hat{h}). \tag{10}$$

Using expansions (8), (9) and (10) the action of $\hat{\mathscr{U}}(t)$, for instance, on a ket state is realised via the action of $Q_m(\hat{h})$ on that ket vector. We thus define the so-called Chebyshev vectors $|\phi_m\rangle = Q_m(\hat{h})|\psi(0)\rangle$ and use the recursive relation of $Q_m(x)$ to write:

$$|\phi_m\rangle = 2\hat{h}|\phi_{m-1}\rangle - |\phi_{m-2}\rangle, \tag{11}$$

with $|\phi_0\rangle = |\psi(0)\rangle$ and $|\phi_1\rangle = \hat{h}|\phi_0\rangle$. This recursive relation of the Chebyshev states is useful to calculate the state $|\psi(t)\rangle$, which is evolved in time from an initial state $|\psi(0)\rangle$ under the action of the time-evolution operator $\hat{\mathscr{U}}(t)$. According to Eq. (8) we obtain the formula:

$$|\psi(t)\rangle = e^{iE_0 t/\hbar} \sum_{m=0}^{+\infty} \frac{2}{\delta_{m,0}+1} (-i)^m B_m \left(\frac{Wt}{\hbar}\right) |\phi_m\rangle. \tag{12}$$

The expectation of the time-evolution operator $\hat{\mathscr{U}}(t)$ measured in the state $|\psi(0)\rangle$ is thus the definition of a time auto-correlation function $C_\psi(t)$:

$$\langle\psi(0)|\hat{\mathscr{U}}(t)|\psi(0)\rangle = \langle\psi(0)|\psi(t)\rangle = C_\psi(t). \tag{13}$$

II.2. Evaluation of traces using stochastic technique

In this subsection, we address a crucial issue of calculating the trace of operators. Denote $\hat{\mathscr{O}}$ a generic operator acting on the Hilbert space defined by a Hamiltonian $\hat{\mathscr{H}}$. Even in the case of finite dimension, said N, at first glance, this task looks far more complicated. Numerically, given a basis, the computational cost is scaled by N^2. It turns out, however, that the stochastic technique can extremely facilitate the trace calculation. Indeed, if defining a ket vector

$$|\psi_r\rangle = \sum_{i=1}^{N} g_{rj}|j\rangle, \tag{14}$$

where $\{|j\rangle\}$ are a basis and $\{g_{rj}\}$ is a set of independent identically distributed random complex variables, which in terms of the statistical average $\langle\langle\ldots\rangle\rangle$ fulfill

$$\langle\langle g_{ri}\rangle\rangle = 0, \tag{15}$$

$$\langle\langle g^*_{ri} g_{r'j}\rangle\rangle = \delta_{rr'}\delta_{ij} \tag{16}$$

then it is straightforwards to show that

$$\langle\langle O_r\rangle\rangle = \sum_{j=1}^{N} O_{jj} = \mathrm{Tr}\left[\hat{\mathscr{O}}\right]. \tag{17}$$

where $O_r = \langle\psi_r|\hat{\mathscr{O}}|\psi_r\rangle$ and O_{ij} are the elements of $\hat{\mathscr{O}}$ in the basis $\{|i\rangle\}$, namely $O_{ij} = \langle i|\hat{\mathscr{O}}|j\rangle$. Eq. (15) therefore shows that if there is a set of R vectors $|\psi_r\rangle$ defined as above, we can evaluate the trace of $\hat{\mathscr{O}}$ by a stochastic average:

$$\mathrm{Tr}\left[\hat{\mathscr{O}}\right] \approx \frac{1}{R}\sum_{r=1}^{R} \langle\psi_r|\hat{\mathscr{O}}|\psi_r\rangle. \tag{18}$$

This result establishes an efficient scheme for calculating the trace of operators because the number R of random states does not scale with the dimension N of the Hilbert space. Practically, this number R can be kept constant or even reduced with increasing N. In Ref. [28] Iitaka and Ebisuzaki showed an expression for the accuracy of this stochastic scheme. It was shown that the distribution

of the elements of $|\psi_r\rangle$, $p(g_{rj})$, has a slight influence on the precision of the estimation Eq. (19). Consequently, the set of $\{g_{rj}\}$ generated as random phase factors, *i.e.,* $g_{rj} = e^{i\phi_{rj}}$ where $\phi_{rj} \in [0, 2\pi]$, is the possible choice for the stochastic trace estimation [27].

II.3. Sampling of localized states and local density of states

In the previous subsection, we generally show that using a set of random phase states can help to evaluate efficiently the trace of operators acting in a large dimension Hilbert space. To unveil the physics of electrons at the atomic scale it is, however, useful to invoke localized states, e.g., atomic orbitals or Wannier-like functions in general, to represent generic electron states. This approach leads to the so-called tight-binding formalism for the electronic structure of atomic lattices. Besides the capability of providing the electronic characteristics of an atomic lattice, *e.g.* local density of states (LDOS) and the distribution of electron density at lattice nodes, the tight-binding formalism is powerful in computation compared to other methods based on the Bloch theorem since they need to analyze symmetries of lattice in detail.

Given an atomic lattice, for the sake of simplicity, we assume that each atom provides only one valence electron occupying a state localised at the atom position, say $|j\rangle$, where j denotes the order of atom in the lattice. The idea of the tight-binding formalism is the use of these localised states as a basis to represent generic electron states. In general, an electron state at a time t can be written in the basis of $\{|j\rangle, j = 1, 2, \ldots, N\}$ as follows

$$|\psi(t)\rangle = \sum_{j=1}^{N} g_j(t)|j\rangle, \tag{19}$$

where $g_j(t)$ is the probability amplitude of finding electron at lattice node j at time t. The quantity $P_j(t) = |\langle j|\psi(t)\rangle|^2 = |g_j(t)|^2$ is thus the probability density determining the dynamics of an electron in the lattice. In principle, the value of $g_j(t)$ is obtained by solving the time-dependent Schröedinger equation but equivalently, the calculation is performed via Eq. (12).

Eq. (14) with $g_{rj} = e^{i\phi_{rj}}$ provides a general manner to generate a set of random phase state vectors to evaluate the operator trace. In our work, we follow a different strategy instead. Accordingly, we chose a lattice node randomly, then select the corresponding interested orbital to be the initial state $|\psi(t = 0)\rangle$. It means that we choose the coefficients $g_j(t = 0) = \delta_{ij}e^{i\phi}$, where ϕ is a random real number, and thus

$$|\psi(t = 0)\rangle = \sum_{j=1}^{N} \delta_{ij}e^{i\phi}|j\rangle = e^{i\phi}|i\rangle. \tag{20}$$

This choice allows us defining the local time-autocorrelation function

$$C_i(t) = \langle i|\psi(t)\rangle. \tag{21}$$

Using Eq. (19) it yields $C_i(t) = \langle i|\psi(t)\rangle = g_i(t)$, *i.e.*, equal to the local probability amplitude at the node i. Its power spectrum, defined as the Fourier transform of $C_i(t)$, is identified as the density of states of an electron at the lattice node i, *i.e.,* the local density of states [20, 27]:

$$\rho_i(E) = \frac{s}{\pi\hbar\Omega_a}\mathrm{Re}\left[\int_0^{+\infty} dt e^{iEt/\hbar}C_i(t)\right] \tag{22}$$

The time-autocorrelation function $C(t)$, and the global density of states $\rho(E)$, are thus calculated by averaging local information. Particularly, from Eq. (18) we learn that these quantities can be well approximated by an ensemble average of $C_i(t)$ and $\rho_i(E)$ over a small set of sampled localized states $|i\rangle$ [20]. This calculation technique is powerful because it works for generic lattices with or without the translational symmetry. For the lattices with the translational symmetry, the complete set of sampled lattice nodes includes all lattice nodes in the primitive cell. The number of such nodes is usually not too large. In this case, the calculation procedure for $C(t)$ and $\rho(E)$ is exact. For the lattices without the translational symmetry, we have to, in principle, work with a set of a large number of sampled lattice nodes to ensure the reliability of the ensemble average value. Practically, as will be shown in the discussion section, a modest large number of sampled lattice nodes is sufficient to approximately obtain the values of $C(t)$ and $\rho(E)$. In next sections, we will present the results by employing Eqs. (20), (11), (12), (21), (22), and (18) to determine the electronic structure of several configurations of the twisted bilayer graphene system.

II.4. Tight-binding Hamiltonian for valence electrons in bilayer graphene

To employ the calculation method presented in the previous subsections to study the electronic structure of the twisted bilayer graphene we need to specify a Hamiltonian defining the dynamics of electrons. It is well-known that in graphene, and generally graphite, the electronic properties are governed by electrons that occupy the $2p_z$ orbitals of carbon atoms (the other orbitals contribute to the strong σ bonds between carbon atoms, governing the planar structure of graphene). The hybridization of the $2p_z$ orbitals forms the π-bond between carbon atoms. Accordingly, we use the tight-binding approach to specify the Hamiltonian for the $2p_z$ electrons in the TBG system [20]:

$$\mathscr{H}_{\text{TBG}} = \sum_{\nu=1}^{2}\left[\sum_{i,j} t_{ij}^{\nu}\hat{c}_{\nu i}^{\dagger}\hat{c}_{\nu j} + \sum_{i} V_i^{\nu}\hat{c}_{\nu i}^{\dagger}\hat{c}_{\nu i}\right] + \sum_{\nu=1}^{2}\sum_{ij} t_{ij}^{\nu\bar{\nu}}\hat{c}_{\nu i}^{\dagger}\hat{c}_{\bar{\nu} j}. \tag{23}$$

In this Hamiltonian, the terms in the square bracket define the hopping of the $2p_z$ electrons in a monolayer of graphene. The layer is labeled by the index ν. The ket vectors of the basis set for this representation are therefore denoted by $\{|\nu, i\rangle\}$. The intra-layer hopping energies of electron between two lattice nodes i and j are denoted by t_{ij}^{ν}. V_i^{ν} are the onsite energies that are generally introduced to include local spatial effects. The dynamics of an electron in the lattice is described via the creation and annihilation of an electron at a layer "ν" and a lattice node "i" through the operators $\hat{c}_{\nu i}^{\dagger}$ and $\hat{c}_{\nu i}$, respectively. The last term in Eq. (23) describes the hopping of electron between two layers which is characterized by the hopping parameters $t_{ij}^{\nu\bar{\nu}}$. The notation $\bar{\nu}$ implies that $\bar{\nu} \neq \nu$. We use the following model to determine the values of the hopping parameters t_{ij}^{ν} and $t_{ij}^{\nu\bar{\nu}}$ [29,30]:

$$t_{ij} = V_{pp\pi}^{0}\exp\left(-\frac{R_{ij}-a_{\text{cc}}}{r_0}\right).\left[1-\left(\frac{\mathbf{R}_{ij}.\mathbf{e}_z}{R_{ij}}\right)^2\right] + V_{pp\sigma}^{0}\exp\left(-\frac{R_{ij}-d}{r_0}\right).\left(\frac{\mathbf{R}_{ij}.\mathbf{e}_z}{R_{ij}}\right)^2. \tag{24}$$

In this model we use two Slater-Koster parameters $V_{pp\pi} \approx -2.7$ eV and $V_{pp\sigma} \approx 0.48$ eV that determine the coupling energies of the $2p_z$ orbitals via the π and σ bonds. These parameters characterise the hybridisation of the nearest-neighbour $2p_z$ orbitals in the intra-layer and inter-layer graphene sheets, respectively. The exponential factors describe the decay of the hopping

energies with respect to the distance. The empirical parameter r_0 is used to characterise the decay of the electron hopping. It is estimated to be $r_0 \approx 0.184\sqrt{3}a_{\rm cc}$ where $a_{\rm cc} \approx 1.42$Å is the distance between two nearest carbon atoms. The scalar products of the vector $\mathbf{R}_{ij}$ connecting two lattice nodes i and j and the unit vector $\mathbf{e}_z$ defining the z direction perpendicular to the graphene surface accounts for the angle-dependence of the orbital coupling. From Eq. (24) we see that when i and j belong to the same layer, $\mathbf{R}_{ij}$ is perpendicular to $\mathbf{e}_z$ so that we obtain the intra-layer hopping $t_{ij}^{\nu} = V_{pp\pi}\exp[-(R_{ij}-a_{\rm cc})/r_0]$, otherwise we get $t_{ij}^{\nu\bar{\nu}}$. In this work, for simplicity we ignore effects of the graphene sheet curvature [31, 32]. We thus assume the spacing between the two layers is about $d \approx 3.35$Å and set the onsite energies V_i^{σ} to be zero.

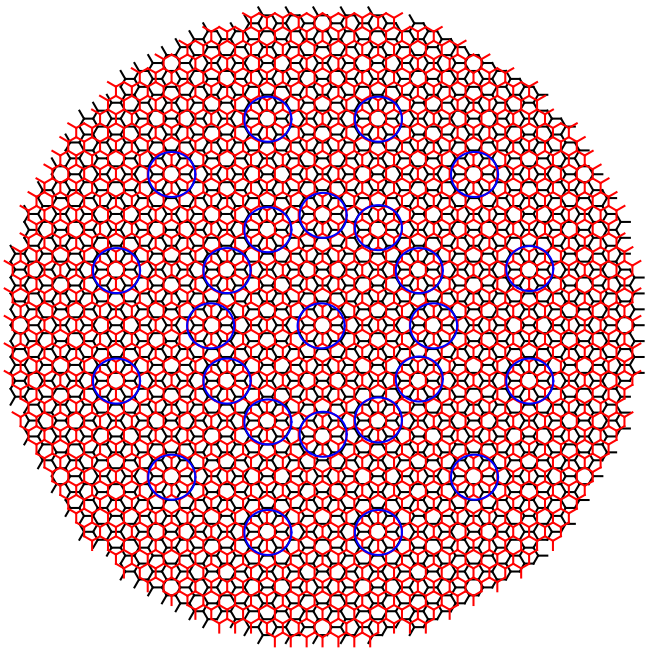

Fig. 1. Atomic configuration of the twisted bilayer graphene with the twist angle of 30°. The twisting axis is perpendicular to the lattice plane and goes through the center of the hexagonal ring of carbon atoms. This axis is also the 12-fold rotational symmetry element. The atomic lattice shows the formation of patterns similar to the six-petal flowers; some of which are remarked by the blue circles to highlight the 12-fold rotational symmetry.

III. RESULTS AND DISCUSSION

III.1. Discussion of computational technique

We discuss in this subsection essential technical issues involving the implementation of the method presented above. First of all, let's discuss how to realize the action of a Hamiltonian $\hat{\mathscr{H}}$ on an electron state. In principle, in terms of $2N$ basis vectors $\{|\nu, j\rangle, \nu = 1,2; j = 1,\ldots,N\}$ an electronic state of TBGs and the Hamiltonian are represented by a $2N$-dimension vector and a

$2N \times 2N$ matrix, respectively. The action of $\hat{\mathscr{H}}$ on a state $|\psi\rangle$ should not be implemented simply by taking the conventional matrix-vector multiplication. We should notice that the tight-binding Hamiltonian is a sparse matrix because of the rapid decay of the electronic hopping parameters. Additionally, since $c^{\dagger}_{\nu i}c_{\delta j}|\mu,k\rangle = \delta_{\mu\delta}\delta_{jk}|\nu,i\rangle$, we directly obtain an expression for the matrix-vector action $\hat{\mathscr{H}}|\nu,j\rangle$ as follows:

$$\hat{\mathscr{H}}|\nu,j\rangle = \sum_{i(j)} t^{\nu}_{ij}|\nu,i\rangle + V^{\nu}_{j}|\nu,j\rangle + \sum_{i(j)} t^{\bar{\nu}\nu}_{ij}|\bar{\nu},j\rangle, \tag{25}$$

where the sum over the i index is taken over the lattice nodes around the node j. Numerically, the realization of this equation is straightforward. The number of arithmetic operations needed for the $\hat{\mathscr{H}}|\psi\rangle$ action is linearly scaled by the dimension number of the state vectors, i.e., $\mathscr{O}(2N)$, rather than $\mathscr{O}((2N)^2)$ of the conventional matrix-vector multiplication.

Next, we address on the rescaling of the Hamiltonian. To do so, we first determine the spectrum width W of $\hat{\mathscr{H}}$. We use the power method for the estimation of the largest absolute eigenvalue of $\hat{\mathscr{H}}$. Starting from a vector $|b_1\rangle = |\nu,j\rangle$ we generate a series of vectors $|b_k\rangle = \hat{\mathscr{H}}|b_{k-1}\rangle$ and then calculate the quantities $\mu_k = \langle b_k|\hat{\mathscr{H}}|b_k\rangle / \langle b_k|b_k\rangle$. By checking the convergence of the series μ_k we can obtain the value of $|\lambda_{max}| \approx \mu_k$. The spectrum width W of $\hat{\mathscr{H}}$ is hence chosen to be slightly larger than $2|\lambda_{max}|$ to ensure that the spectrum of $\hat{h}$ completely lies in the interval $(-1,1)$. The value of W should not be chosen much largely than $2|\lambda_{max}|$ because if it is, the spectrum width of $\hat{h}$ become too narrow. The energy resolution η therefore requires to be refined. It thus leads to the increase of the numerical computational cost.

The two technical points discussed above are practically invoked to calculate a series of Chebyshev vectors $|\phi_m\rangle$ using Eq. (11) with the starting state $|\phi_1\rangle = |\nu,j\rangle$. We should notice that, though Eq. (12) is exact, we cannot numerically implement the summation of an infinite series of terms. We, therefore, have to approximate it by making a truncation, keeping M first important terms. Together with the approximation of the finiteness of the Hilbert space of $2N$-dimension, we now discuss the effects of the two computational parameters N and M.

We present in Fig. 2 the variation of the time-autocorrelation function $C_{\nu j}(t)$ obtained for three square samples of the AB-stacking system of the size $L = 100$, 200 and 300 nm. These samples contain the total ($2N$) number of lattice nodes of 1 527 079, 6 108 315, and 13 743 708, respectively. For each sample, we display the function $C_{\nu j}(t)$ resulted from the calculation using three different values $M_1 < M_2 < M_3$ for the number of the Chebyshev expansion terms in Eq. (12). The red, blue and green curves are for M_1, M_2 and M_3, respectively. We observe that the obtained data for $C_{\nu j}(t)$ behave the oscillation with respect to time. The red curve is coincident with the blue curve in a short evolution time range, and the blue curve is coincident with the green curve in a longer evolution time range. These numerical calculation data obviously demonstrate the fact that keeping as many as possible the Chebyshev terms in Eq. (12) validates the evolution of electronic states in a large time range. However, we find that the evolution time range cannot be infinitely enlarged by increasing M. When M is increased to a certain value, said M_{cutoff}, it leads to the unphysical behavior of $C_{\nu j}(t)$ as the increase of the oscillation amplitude after a certain time, said t_{cutoff}. Continuously increasing M does not prolong t_{cutoff}. M_{cutoff} is thus the minimal value that defines the longest t_{cutoff}. Data are shown in Fig. 2, however, reveals that both t_{cutoff} and M_{cutoff} can be increased by enlarging the sample size L. We performed the calculation for a series of samples of different size to collect data for the relationship of M_{cutoff} and L and of t_{cutoff}

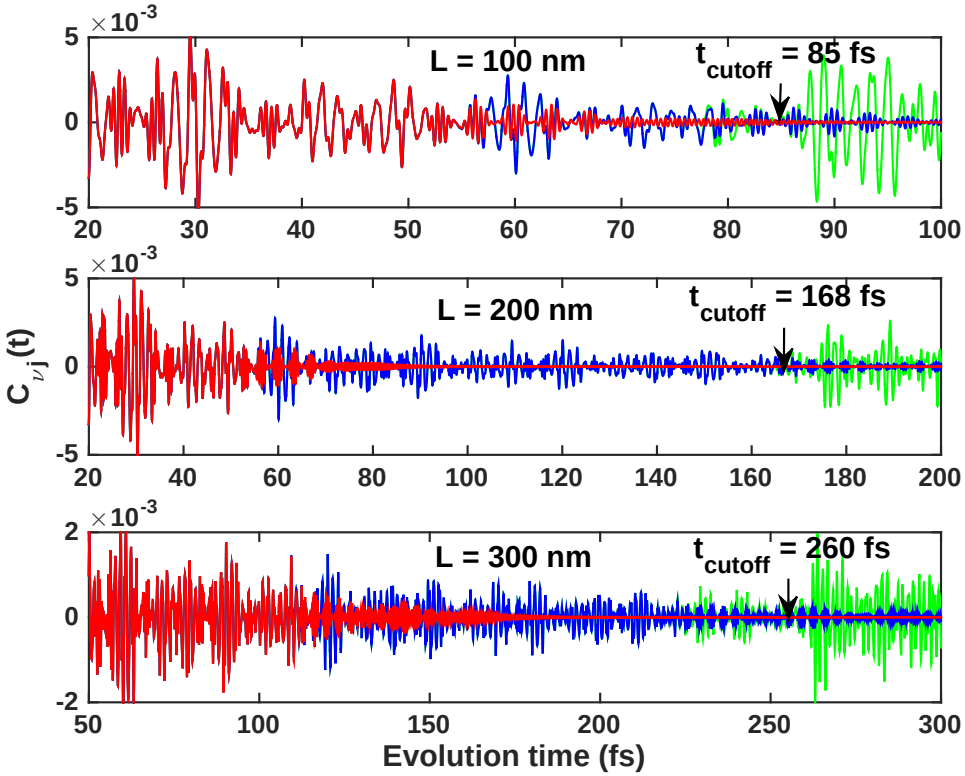

Fig. 2. The time auto-correlation function $C(t)$ calculated for three square AB samples of different size. For the sample with $L = 100$ nm, the curves in red, blue and green are obtained for $M = 1001, 1501$ and 3001, respectively. For the sample with $L = 200$ nm, the curves in red, blue and green are obtained for $M = 1001, 3001$ and 5001, respectively. For the sample with $L = 300$ nm, the curves in red, blue and green are obtained for $M = 2001, 4001$ and 6001, respectively. The time cutoff for the three samples is determined to be about 85, 168 and 260 fs, respectively.

and M_{cutoff}. In Fig. 3 we display the obtained data. The figure clearly shows the linear law with the slope factors of 0.066 for the $L - M_{cutoff}$ line and 0.057 for the $t_{cutoff} - M$ line. These results show the linearly scaled cost $\mathscr{O}(N)$ of the presented method.

The unphysical behavior of $C_{\nu j}(t)$ must be removed in the calculation of physical quantities. For the local density of states $\rho_{\nu j}(E)$, for instance, according to Eq. (22) we have to deal with an infinite integral over time. Theoretically, a factor of $\exp(-\eta t)$ is usually introduced to ensure the convergence of the integral. In fact, with an appropriate positive value of η, this factor is a decay function of $t > 0$, so it plays the role of eliminating the contribution of $C_{\nu j}(t)$ at large t to the integral value. Physically, the value of η should be in the order of the energy resolution, about 10^{-3} eV, but this value is too small to suppress the behavior of $C_{\nu j}(t)$. Practically, in order to suppress the unphysical behavior of $C_{\nu j}(t)$ after $t > t_{cutoff}$, we usually need a much larger value for η. In Fig. 4 we display the behaviour of the function $C_{\nu j}(t)$ multiplied by the factor

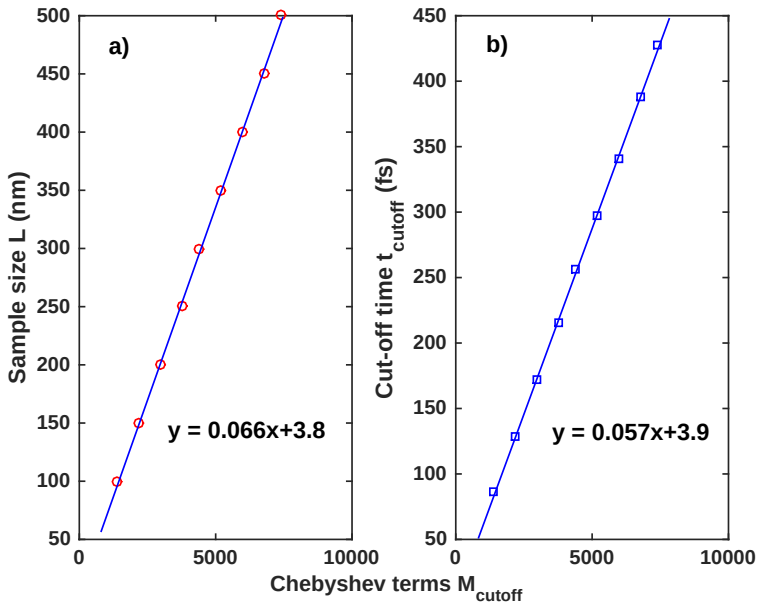

Fig. 3. The linear dependence of (a) the number of Chebyshev terms M on the sample size L, and (b) the cut-off evolution time t_{cutoff} on the number of Chebyshev terms M. The blue lines denote the fitting lines with the equations shown in the corresponding panels.

$\exp(-\eta t)$ with $\eta = 3\times10^{-2}$, see the green curve. Another scheme for eliminating the unphysical behavior of $C_{vj}(t)$ at large evolution time is to use the factor of $\exp(-\delta t^2)$ [33]. This factor is a function decaying much more rapidly than the one $\exp(-\eta t)$. However, it results in the strong reduction of oscillation amplitude of this function in the range of $t < t_{cutoff}$ (see the blue curve in Fig. 4 with $\delta = 2\times10^{-2}$). Consequently, it yields a less accurate value for the local density of states. In our calculation, instead of introducing a factor like $\exp(-\eta t)$ or $\exp(-\delta t^2)$ we use the Heaviside function $\theta(t_{cutoff} - t)$ to truncate the contribution of $C_{vj}(t)$ from $t > t_{cutoff}$. This technique actually transforms Eq. (22) from the infinite integral into a definite one with the upper limit t_{cutoff}. In principle, we need to enlarge the value of t_{cutoff} to obtain the value of $\rho_{vj}(E)$ as much precise as possible. To compromise the accuracy of the calculation and the computational time and computer resources, the results presented in Fig. 3 are the thumb rule for setting the value for the two computation parameters L and M and for estimating t_{cutoff}.

The dependence of $C_{vj}(t)$ on M and L can be physically understood. Indeed, the replacement of the infinite expansion of the time-evolution operator $\hat{\mathscr{U}}(t)$ by a finite sum beaks the unitary property of this operator. It results in the non-preservation of the probability conservation, i.e. the vector norm. This loss is one of the origins of the unphysical behavior of $C_{vj}(t)$. Another important origin lies in the finiteness of lattice samples used to perform the calculation. Physically, assuming the initial state $|\psi(t=0)\rangle$ localizes at a lattice node in the center of a sample, under the action of $\hat{\mathscr{U}}(t)$ the wave develops and spreads over the sample to the edges. The periodic and

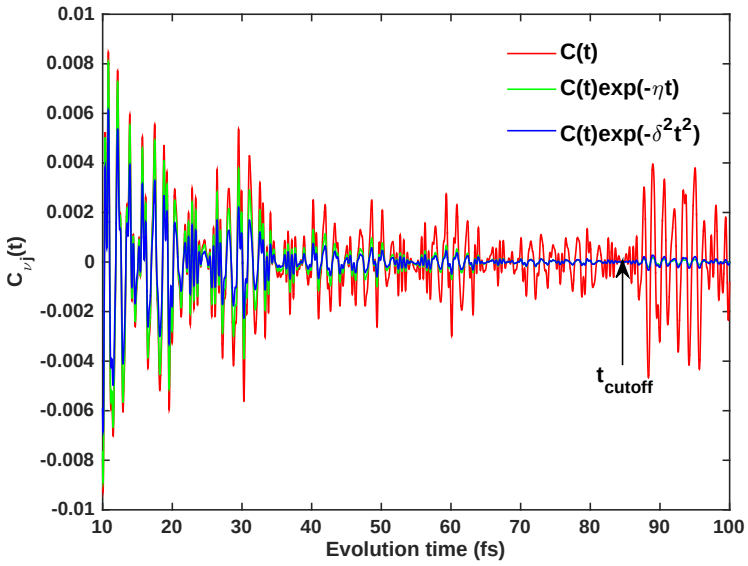

Fig. 4. The modification of the original time auto-correlation function $C_{\nu j}(t)$ (the red curve) to eliminate the unphysical behaviour for $t > t_{cutoff}$. The green and blue curves are obtained by multiplying $C_{\nu j}(t)$ with the weight factors $\exp(-\eta t)$ with $\eta = 3\times 10^{-2}$, and $\exp(-\delta^2 t^2)$ with $\delta = 2\times 10^{-2}$, respectively.

rigid boundary conditions result in the same effect that the value of the wave at a lattice node inside the sample is multiple times contribute due to the wave reflection. Increasing the sample size, it increases the time that the wave reaches the edges and thus weaken the effects of the reflection.

III.2. Electronic structure and charge distribution in a quasi-crystalline bilayer graphene

In this subsection, we first validate the correctness and the efficiency of the presented method for the DOS calculation. We will present and discussed data for a familiar and typical bilayer graphene system before doing with the generic twisted bilayer graphene system.

Figure 5 shows the density of states of electrons in the AB-stacking configuration. This is a special configuration of the bilayer graphene in the meaning that the stacking is commensurate and the atomic lattice is defined by a unit cell with the smallest area of $3\sqrt{3}a_{cc}^2$. The cell contains only 4 inequivalent lattice nodes A_1, B_1, A_2 and B_2. Here A_2 is on top of B_1, and B_2 is on the position of the center of the hexagonal ring A_1-B_1 of the bottom graphene layer. The electronic structure of the AB-stacking configuration was commonly studied by various methods, including the ones based on first principles and on empirical pseudo-potential and tight-binding models [34]. For the aim of validating the data obtained by the presented method here, we calculated the DOS of the AB-stacking configuration by exactly diagonalizing Hamiltonian (23). The obtained data are presented in Fig. 5 as the thick pink curve. The figure shows the consistency of the data obtained by two methods. It should be noted that the blue curve is obtained by averaging over the local density of states $\rho_{\nu j}(E)$ at 4 atomic sites in the unit cell, i.e., $\nu = 1,2$ and $j = 1,2$. Computationally, in order to obtain $\rho_{\nu j}(E)$ we need to perform an integral over only the time variable of the time

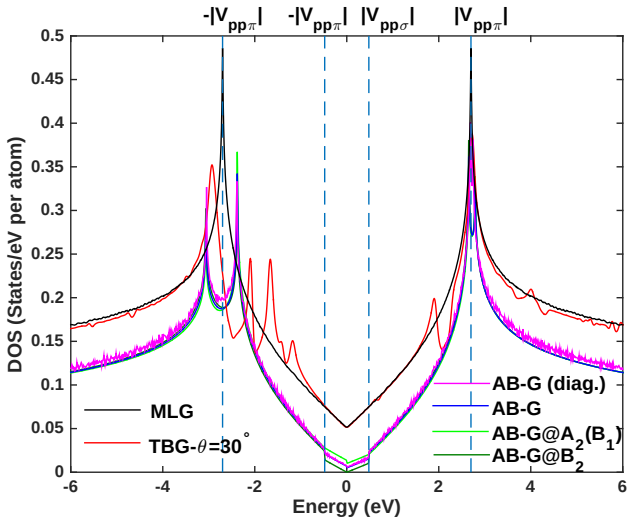

Fig. 5. The density of states of electrons in the AB-stacking bilayer graphene (the blue and pink curves) and in the TBG configuration with the twist angle $\theta = 30^\circ$ (the red curve, which is shifted upward to separate the curves). The green and moss-green curves respectively are the local density of states in the AB-system at the lattice nodes A_2 (on top of the B_1 node) and B_2 on the center of the $A_1 - B_1$ hexagonal ring. The black curve is for the monolayer graphene.

correlation function $C_{\nu j}(t)$. Meanwhile, for the exact diagonalization method we need to perform the summation of $\sum_{n,\mathbf{k}} \delta[E - E_n(\mathbf{k})]/N_\mathbf{k}$, where $n = 1,2,3$ and 4 and $N_\mathbf{k}$ is the number of $\mathbf{k}$ points defined by appropriately meshing the Brillouin zone. Though straightforward, the calculation of the sum over $\mathbf{k}$ is expensive because it requires to approximate the delta-Dirac function. We solved this problem through the retarded Green function. A positive number γ is thus introduced as the spectrum smearing parameter in the Green function. In order to decrease η, *i.e.,* increasing the spectrum resolution, we need to finely meshed the Brillouin zone. The number of the $\mathbf{k}$-points $N_\mathbf{k}$ is therefore very large. Practically, we used $\gamma = 5 \times 10^{-3}$ and $N_\mathbf{k} = 1\,248\,971$. It results in the pink curve with visible fluctuations.

The difference of the local density of states $\rho_{\nu j}(E)$ on the nodes A_2 and B_2 on the same graphene layer ($\nu = 2$) are shown in Fig. 5 as the green and moss-green curves. It is clearly realized that the difference is significant in the energy intervals around the Fermi energy level $E_F = 0$ and the positions of the van Hove singularity peaks, *i.e.,* at $E = \pm|V_{pp\pi}|$, of the energy spectrum of monolayer graphene. In the former energy interval $(-V_{pp\sigma}, V_{pp\sigma})$, the density of states at the A_2 node linearly depends on the energy, and hence vanished at $E_F = 0$ eV, while that at the B_2 node is finite. By decreasing the value of $V_{pp\sigma}$ the density of states at the B_2 node is reduced and approaches to that at the A_2 node. The difference of the local density of states at different atomic nodes obviously is the effect of the interlayer coupling. In other words, it is said that the interlayer coupling causes the inequivalence of the atoms at the A and B lattice nodes in the AB-stacking configuration. It should be noticed that, in this work, we considered only the intra- and inter-layer hopping of electron occurring between carbon atoms in the distance of $r = a_{cc}$ and

$d \leq r < \sqrt{d^2 + a_{cc}^2}$, respectively, *i.e.*, taking only the nearest-neighbor coupling, but it is not the limitation of the presented method. We also calculate the LDOS and DOS of the AA-stacking configuration but do not show and discussed here.

We now discussed the density of states of electrons in the special twisted bilayer graphene with the twist angle of 30°. The data is displayed in Fig. 5 as the red solid curve. We shift it upward to separate the curves. We observe the appearance of many sub-peaks of DOS in the energy ranges around $\pm|V_{pp\pi}|$, i.e., containing the two van Hove peaks of DOS of the monolayer graphene (the black curve). The appearance of many DOS-peaks can be elucidated as the result of the folding of energy surfaces due to the enlarging of the unit cell of the TBG lattice in comparison with the AB-stacking configuration. It also reflects the effect of the interlayer coupling, not in the whole, energy range, but in certain narrow ones. Different from the case of AB-stacking configuration, the DOS of the $\theta = 30^\circ$ TBG configuration in the energy range around the charge neutrality level $E_F = 0$ is coincident with that of monolayer graphene. These behaviors suggest that in the TBG configuration, the interlayer coupling does not manifest uniformly in the whole energy range, but dominant in the energy range around $\pm|V_{pp\pi|}$, and less in the range of $[-V_{pp\sigma}, V_{pp\sigma}]$. It should be remembered that the atomic lattice of this TBG configuration is quasi-crystalline, see Fig. 1. The electronic structure of this configuration, however, has not yet theoretically studied because the lattice has no translational symmetry. Though the electronic structure of the TBG configurations with modest and tiny twist angles has been studied, it was usually realized using the exact diagonalization method for commensurate configurations. In these cases, the atomic lattices can be defined by a unit cell but it is usually large, containing a large number of inequivalent lattice nodes inside. One should note that the cost of diagonalizing a matrix is $\mathcal{O}((2N)^3)$, where $2N$ denotes the matrix size. It means that the conventional approach is really expensive. Meanwhile, the calculation based on effective models though efficient is just applicable in the approximation of long wavelength. It thus ignores, in general, the discrete nature of the TBG lattice.

One of the strong points of the presented method is the potential to calculate local information of an electronic system in real space. Particularly, we obtained the local density of states $\rho_{\nu j}(E)$ of electron on a set of about 450 lattice nodes of the TBG configuration with $\theta = 30^\circ$. The data shows the variation of $\rho_{\nu j}(E)$ from node to node. It suggests a fluctuation of the electron density on the lattice nodes. We thus performed the calculation for the electron density $n^e_{\nu j}$ on each lattice node using the formula:

$$n^e_{\nu j} = \int_{-\infty}^{+\infty} dE \rho_{\nu j}(E) f\left(\frac{E - E_F}{k_B T}\right) = \int_{-\infty}^{E_F} dE \rho_{\nu j}(E), \tag{26}$$

where $f(x)$ is the Fermi-Dirac function which determines the occupation probability of electrons in a state with energy E. The last equation is given in the limit of zero temperature due to the step feature of the Fermi-Dirac function. The fluctuation of the electron density is then obtained by $\delta n^e_{\nu j} = n^e_{\nu j} - \langle n^e_{\nu j} \rangle$, where $\langle n^e_{\nu j} \rangle$ is the average value. In Fig. 6 we present the obtained result. We use the blue/green solid circles to denote the nodes with $\delta n^e_{\nu j} > 0$ and the red/black empty circles for the nodes with $\delta n^e_{\nu j} < 0$. The radius of these circles is proportional to the value of $n^e_{\nu j}$. Surprisingly, we observe a typical pattern of the electron density fluctuation on the atomic lattice of the considered TBG configuration. The pattern of the hexagonal ring of $\delta n^e_{\nu j} < 0$ is formed consistently with the atomic pattern of the TBG lattice seen in Fig. 1. This interesting result

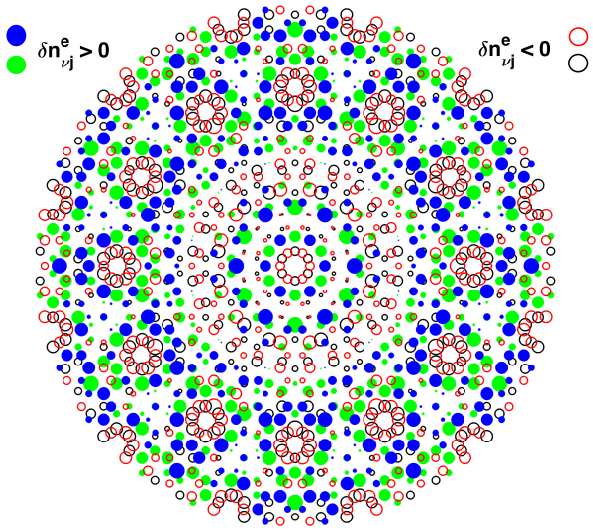

Fig. 6. Distribution of the electron density fluctuation $\delta n^e_{\nu j} = n^e_{\nu j} - \langle n^e_{\nu j} \rangle$ ($\nu = 1,2$) on the lattice nodes of the quasi-crystal TBG configuration with the twist angle of 30°. The red/black-empty and blue/green-solid circles denote the nodes at which $\delta n^e_{1/2j} < 0$ and $\delta n^e_{1/2j} > 0$, respectively.

may suggest further studies of the electronic effects on other physical properties, for instance, the adhesion between the two graphene layers.

IV. CONCLUSIONS

We have presented a calculation technique that is generic and powerful to determine efficiently the electronic properties of materials in which the long-range order of atoms arrangement may be broken. The essence of the presented method lies in the analysis of the evolution in time of electronic states in the atomic lattice of considered systems. Technically, the method is based on a three-point scheme. The first point is to represent a physical quantity in term of an appropriate time correlation function, which is usually defined as the projection of a time-dependent state onto another one. The second point is the use of Chebyshev polynomials to specify the time evolution operator. The third point is the employment of a stochastic technique to evaluate the trace of Hermitian operators. For the last point, we proposed an algorithm of sampling states localizing at the atomic positions for the evaluation of trace, instead of using random phase states as initial states. This algorithm allows obtaining the local information of the electronic system as the local time auto-correlation functions and the local density of states. We discussed important technical issues involving the implementation of the method through the calculation of the electronic structure of the bilayer graphene system. We showed the linear scaling law of the computational cost. We calculated the density of states and the electron density in a special twisted bilayer graphene configuration with the quasi-crystalline atomic structure. We observed the formation of many peaks in the picture of DOS as the result of the strong coupling of two graphene layers in the energy ranges containing the two van Hove peaks of DOS in the case of monolayer graphene. In the

energy range around the charge neutrality level, the DOS of the $\theta = 30^\circ$ TBG configuration is identical to the one of graphene. It implies the effective decoupling of Dirac fermions in the two graphene layers. We found a pattern of the fluctuation of the electron density on the TBG configuration. This interesting finding may suggest further studies of physical properties of the considered special quasi-crystalline TBG configuration.

ACKNOWLEDGMENT

The work is supported by the National Foundation for Science and Technology Development (NAFOSTED) under Project No. 103.01-2016.62.

REFERENCES

[1] A. K. Geim and I. V. Grigorieva, *Nature* **499** (2013) 419.
[2] M. Xu, T. Liang, M. Shi and H. Chen, *Chem. Rev.* **113** (2013) 3766.
[3] J. M. B. L. dos Santos, N. M. R. Peres and A. H. C. Neto, *Phys. Rev. Lett.* **99** (2009) 256802.
[4] J. M. L. dos Santos, N. M. R. Peres and A. H. C. Neto, *Phys. Rev. B* **86** (2012) 155449.
[5] R. Bistritzer and A. H. MacDonald, *Proc. Natl. Acad. Sci. U.S.A.* **108** (2011) 12233.
[6] A. V. Rozhkov, A. O. Sboychakov, A. L. Rakhamanov and F. Nori, *Phys. Rep.* **648** (2016) 1.
[7] M. Koshino, N. F. Q. Yuan, T. Koretsune, M. Ochi, K. Kuroki and L. Fu, *Phys. Rev. X* **8** (2018) 031087.
[8] A. O. Sboychakov, A. V. Rozhkov, A. L. Rakhmanov and F. Nori, arXiv:1807.08190.
[9] H. C. Po, L. Zou, A. Vishwanath and T. Senthil, *Phys. Rev. X* **8** (2018) 031089.
[10] D. M. Kennes, J. Lischner and C. Karrasch, *Phys. Rev. B* **98** (2018) 241407(R).
[11] K. Kim, A. DaSilva, S. Huang, B. Fallahazad, S. Larentis, T. Taniguchi, K. Watanabe, B. J. LeRoy, A. H. MacDonald and E. Tutuc, *PNAS* **114** (2017) 3364.
[12] F. Guinea and N. R. Walet, *PNAS* **115** (2018) 13174.
[13] Y. Cao, V. Fatemi, S. Fang, K. Watanabe, T. Taniguchi, E. Kaxiras and P. Jarillo-Herrero, *Nature* **556** (2018) 43.
[14] Y. Cao, V. Fatemi, A. Demir, S. Fang, S. L. Tomarken, J. Y. Lou, J. D. Sanchez-Yamagishi, K. Watanable, T. Taniguchi, E. Kaxiras, R. C. Ashoori and P. Jarillo-Herrero, *Nature* **556** (2018) 80.
[15] L. Zou, H. C. Po, A. Vishwanath and T. Senthil, *Phys. Rev. B* **98** (2018) 085435.
[16] S. Shallcross, S. Sharma and O. A. Pankratov, *Phys. Rev. Lett.* **101** (2008) 056803.
[17] E. J. Mele, *J. Phys. D: Appl. Phys.* **45** (2012) 154004.
[18] A. V. Rozhkov, A. O. Sboychakov, R. A. L. and F. Nori, *Phys. Rev. B* **95** (2017) 045119.
[19] J. Rode, D. Smirnov, C. Belke, H. Schmidt and R. J. Haug, *Ann. Phys.* **1** (2017) 1700025.
[20] H. A. Le and V. N. Do, *Phys. Rev. B* **97** (2018) 125136.
[21] D. Weckbecker, S. Shallcross, M. Fleischmann, N. Ray, S. Sharma and O. Pankratov, *Phys. Rev. B* **93** (2016) 035452.
[22] X. Lin and D. Tománek, *Phys. Rev. B* **98** (2018) 081410(R).
[23] V. N. Do, H. A. Le and D. Bercioux, *Phys. Rev. B* **99** (2019) 165127.
[24] E. Koren and U. Duerig, *Phys. Rev. B* **93** (2016) 201404(R).
[25] W. Yao, E. Wang, C. Bao, Y. Zhang, K. Zhang, K. Bao, C. K. Chan, C. Chen, J. Avila, M. C. Asensio, J. Zhu and S. Zhou, *PNAS* **115** (2018) 6928.
[26] P. Moon, M. Koshino and Y.-W. Son, *Phys. Rev. B* **99** (2019) 165430.
[27] A. Weibe, G. Wellein, A. Alvermann and H. Fehske, *Rev. Mod. Phys.* **78** (2006) 275.
[28] T. Iitaka and T. Ebisuzaki, *Phys. Rev. E* **69** (2004) 057701.
[29] P. Moon and M. Koshino, *Phys. Rev. B* **87** (2013) 205404.
[30] M. Koshino, *New. J. Phys.* **17** (2015) 015014.
[31] K. Uchida, S. Furuya, J.-I. Iwata and A. Oshiyama, *Phys. Rev. B* **90** (2014) 155451.
[32] P. Lucignano, D. Alfe, V. Cataudella, D. Ninno and G. Cantele, arXiv:1902.02690v1.
[33] S. Yuan, H. D. Raedt and M. I. Katsnelson, *Phys. Rev. B* **82** (2010) 115448.
[34] V. N. Do, H. A. Le and V. T. Vu, *Phys. Rev. B* **95** (2017) 165130.